Influence of uniaxial deformation on surface morphology and corrosion performance of chromium-based coatings for packaging steel

Jordan Whiteside (Conceptualization) (Formal analysis) (Investigation) (Methodology) (Writing - original draft), Arnoud C.A. de Vooys (Supervision) (Resources) (Writing - review and editing), Elizabeth Sackett (Methodology) (Writing - review and editing) (Supervision), Hamilton Neil McMurray (Conceptualization) (Methodology) (Writing - review and editing) (Supervision)

PII: S0010-938X(21)00428-5

DOI: https://doi.org/10.1016/j.corsci.2021.109662

Reference: CS 109662

To appear in: *Corrosion Science*

Received Date: 10 March 2021

Revised Date: 28 June 2021

Accepted Date: 1 July 2021

Please cite this article as: Whiteside J, de Vooys ACA, Sackett E, McMurray HN, Influence of uniaxial deformation on surface morphology and corrosion performance of chromium-based coatings for packaging steel, *Corrosion Science* (2021), doi: https://doi.org/10.1016/j.corsci.2021.109662

Influence of uniaxial deformation on surface morphology and corrosion performance of chromium-based coatings for packaging steel

Jordan Whiteside[1], Dr Arnoud C.A. de Vooys[2], Dr Elizabeth Sackett[1] and Prof Hamilton Neil McMurray[1] .

[1] Swansea University, Swansea, United Kingdom, [2]TATA Steel Europe, Ijmuiden, The Netherlands

Highlights

- The kinetics of corrosion-driven cathodic disbondment of a model PVB coating adhered to novel chromium (III) metal-oxide-carbide coated steels, post-application of varying levels of uniaxial strain, was investigated using an in-situ scanning Kelvin probe (SKP).
- The Cr(VI) derived coatings were fully resistant to cathodic disbondment pre and post-application of uniaxial strain.
- Cathodic disbondment kinetics increase with the percentage of uniaxial strain applied for Cr(III) derived coatings
- Cathodic driven disbondment rates suppressed with Cr oxide thickness increase, pre and post deformation.
- Changes in coating morphology induced by deformation are assessed using a scanning electron microscope
- Hydrogen evolution kinetics are measured to assess the electrochemical availability of the underlying iron-based substrate post deformation.

Abstract

Chromium-based coatings on steel, cathodically electroplated from Cr(VI) and Cr(III) electrolytes, were studied to compare their corrosion resistance following application of uniaxial strain. An organic overcoat (PVB) was applied to strained samples and an in-situ scanning Kelvin probe technique was used to determine rates of PVB cathodic disbondment. The Cr(VI) derived coatings were fully resistant to cathodic disbondment post-deformation. The Cr(III) derived coatings exhibited increased rates of cathodic disbondment with increasing uniaxial strain. The Kinetics of cathodic disbondment are

explained on the basis of coating morphology produced by deformation, and the exposure of underlying iron. The electrochemical availability of iron is estimated by measuring hydrogen evolution kinetics on cathodically polarised samples.

Keywords: steel; Chromium; Cathodic disbondment; Oxygen reduction; Packaging Steels; Uniaxial Deformation

1. Introduction

"Tin-Free" Packaging steels with chromium/chromium oxide coatings are typically produced by cathodic electrodeposition of a hexavalent chromium based electrolyte [1-3]. The current industry standard electro-chromium coated steel (ECCS) exhibits a duplex coating consisting of a base layer of chromium metal and a superimposing layer of chromium oxide. The ECCS electrolyte bath typically consists of aqueous chromic acid (CrO_3) and sulphuric acid (H_2SO_4). Hexavalent chromium is a known carcinogenic and considered dangerous to workers on the electroplating line[4-5]. Therefore the demand for a similar but safe coating is significant [6]. The coating must be comparable to ECCS in a range of areas to be a successful replacement. The replacement must be non-toxic and offer the capability to be produced on similar tinning lines used for the packaging steel products. It must also offer corrosion resistance to many types of corrosion mechanisms, including, atmospheric corrosion, delamination and filiform corrosion. The coating must have the formability properties to be deep drawn without any effects on the mechanical or electrochemical properties of the substrate or coating. Lastly, the coating must have the adhesion properties for the lacquers and organic overcoats to be applied and offer the barrier layer protection desired.

A prototype alternative to ECCS has been developed, which uses a trivalent chromium-based electrolyte during the electrodeposition process [1,2,7,8]. The coating comprises of mixed chromium metal, chromium oxide and chromium carbide coating, which presents no risks to workers [1,2,7].

Barrier coatings such as polyethylene terephthalate are used in conjunction with chromium coating steels to resist corrosion initiation [9-14]. A corrosion mechanism associated with this coating matrix is cathodic disbondment. Cathodic disbondment can occur on the internal surface of a can when in the presence of a corrosive electrolyte. This corrosive response to a defect in the polymer coating will determine how long the contents of a can remain preserved [9]. Deformation has been shown to reduce the corrosion performance of ECCS [9,10]. Scanning Kelvin probe (SKP) investigations have been investigated for $Cr3^{+}$ based electrolyte coatings and ECCS [1,2]. Reported results show that ECCS is fully resistant to cathodic driven disbondment and filiform corrosion. $Cr3^{+}$ based coatings demonstrated a reduced rate of cathodic disbondment and filiform corrosion when compared to pure iron; however, the initiation of both atmospheric corrosion mechanisms was observed [1]. Increased resistance to the rate of cathodic disbondment occurs when the level of chromium (III) oxide content was increased for Cr (III) coatings. A high Cr (III) oxide thickness demonstrated full resistance to cathodic disbondment, similar to ECCS [2].

A critical aspect in the protection provided by ECCS or any Cr (III) replacement coating, is the ability to withstand mechanical deformation. Packaging steels are used in the two-piece draw and redraw (DRD) can making industry and will be subjected to high values of elongation, including uniaxial strain. Deep drawing deformation may cause deterioration of the coating in the form of thinning and surface cracking, factors which can influence the corrosion performance [9-16]. The Scanning Kelvin Probe (SKP) technique has been widley used to follow the corrosion-driven cathodic delamination of organic coatings from a variety of metallic substrates[1, 2, 15-21]. A method has been developed by Posner et al. to measure cathodic disbondment rates of organic coatings applied over stretch-formed conversion films on galvanised steel. This study showed micro defects could be produced in the conversion film by deformation, which produced higher anodic and cathodic current density values during cyclic voltammetry, compared to non-deformed samples [15]. The SKP showed that the potential difference between corrosively delaminated and intact organic coated areas (the driving force for cathodic disbondment), increased with the degree of deformation. However, no significant increase in the cathodic delamination rate was detected for samples strained up to 15% [15].

The work to be presented here was aimed at determining the extent to which uniaxial deformation (elongation) of ECCS and Cr(III) coated steels affects the cathodic disbondment kinetics of a subsequently applied organic coating (polyvinyl butyral, PVB). Potential distributions within the cathodic delamination localized corrosion cell and rates of organic coating delamination are measured using an in-situ SKP apparatus in conjunction with a Stratmann type experimental setup. A similar approach has recently been used to show relationships between Cr(III) coating parameters and organic coating cathodic delmaiantion rate in undeformed Cr(III) coated systems [2]. Changes in Cr(III) coating morphology and the accumulation of penetrative Cr(III) coating defects with increasing degrees of elongation are followed systematically using a scanning electron microscope (SEM). The exposure and electrochemical availibilty of substrate iron (through penetrative Cr(III) defects) is estimated using ex-situ cathodic polarisation experiments. Finally the observed changes in cathodic delamination rates are correlated with elongation induced Cr(III) coating defect accumulation and iron exposure to provide a full mechanistic understanding of the phenomena involved.

2. Experimental

2.1 Materials

Iron foil of 99.85% purity and 0.9mm thickness was acquired from Goodfellows Cambridge Ltd. ECCS and the Cr(III) coated steel samples were obtained from TATA Steel Packaging Europe. Two Cr(III) coatings were used with different levels of Cr(III) oxide, a low level of 4mg/m^2 and a high level of 19mg/m^2. Chemical compositions of the Cr(III) coated steel and ECCS samples is listed in Table 1. Uncoated packaing steel was used, known as blackplate, which is a low carbon steel with few other significant alloying elements. The typical composition of the substrate is shown in table 2. The blackplate sample was in accordance with the Euronorm standard 10205. Polyvinyl Butyral (PVB) and other chemicals were analytical grade purity and obtained from Sigma Aldrich.

Table 1 Chemical composition (mg.m^{-2}) of ECCS and Cr (III) coated steel from XRF

Sample	Total Chromium (mg.m^{-2})	Chromium Oxide (mg.m^{-2})
High Cr(III) Oxide	182	19
Low Cr(III) Oxide	187	4
ECCS	138	8

Table 2 Chemical composition wt% of packaging steel substrate

Element	**Content**
Carbon, C	0.22 %
Iron, Fe	99.2%
Manganese, Mn	0.16 %
Phosphorous, P	0.01 %
Sulphur, S	0.01 %
Chromium, Cr	0.02%

2.2 Surface characterisation

Surface morphology studies of the samples were carried out on the JEOL 7800 FEG SEM (Field Emission Gun, Scanning Electron Microscope). Images were captured using the LED (Lower Electron Detector) at a working distance of between 7-8 mm and an accelerating voltage of 5kv.

2.3 Application of Uniaxial Deformation

The samples were uniaxially deformed to 5%, 10% and 20% strain using a Hounsfield/Tinius Olsen tensile tester and extensometer. A typical stress-strain curve of a Cr(III) coated steel samples, shown in Fig.2, identifties the elongation points of the strain values chosen. The tensile samples were dog-bone shaped and had a gauge area of 60 x

$22mm^2$ (Fig.3). A 30mm extensometer was used to measure the elongation values of the tensile samples. The degree of deformation percentage corresponds to the sample elongation along the long axis.

2.4 Electrochemical Characterisation

Cathodic Polarisation

Cathodic polarisation electrochemical experiments were conducted using a Solartron 1280 Electrochemical Measurement Unit. Mercury-Mercury Sulphate Reference Electrode, in conjunction with a three-electrode cell, was used to provide a fixed potential throughout the experiment. Coated steel samples were cut to discs of 20mm diameter and placed in a working electrode sample holder, exposing a substrate area of 10mm diameter to the electrolyte. Tests were completed in a 0.5 M aqueous sodium sulphate (Na2SO4) containing 0.025 M sodium tetraborate ($Na_2B_4O_7.10H_2O$) and 0.1 M sodium hydroxide (NaOH), which gave a buffered solution of pH9.3 at 20^{o}C. Deaerated conditions were used and achieved by a nitrogen purge for 30 minutes before each experiment. During the scan, nitrogen flowed over the surface of the electrolyte and then the electrolyte covered to maintain deaerated conditions. Potentiodynamic scans were completed at a scan rate of 0.333 mv/s and using a platinum gauze counter electrode. Under deaerated conditions, the principal cathodic reaction will be hydrogen evolution. Cathodic hydrogen evolution is not thought to be important in the cathodic disbondment of organic coatings from iron/steel. Hydrogen evolution rates are used here merely as a measure of what fraction of the steel substrate is exposed to electrolyte and analysed to support interfacial electron transfer processes.

Cathodic Delamination

For cathodic disbondment experiments the preparation of the samples followed a well-established methodology [1-2,16-21]. Fig.1. displays a representation of the sample preparation. Strained tensile specimens of the coated steels were cut into 30x20mm samples using a sheet metal guillotine. The samples were sectioned from the region measured by the extensometer (Fig.3). All samples were degreased before any experimentation. Adhesive clear tape, measuring 12mm x 20mm was placed over one edge

of the sample, followed by two strips of PVC tape with a thickness of 50µm, placed adjacently to either side of the clear tape. Exposed on the sample was a central 10mm strip of the uncovered surface. PVB solution was used as the model organic coating during the cathodic delamination study. Using a glass rod, the samples were bar coated with a 15% w/w PVB and ethanol solution. The PVB coating thickness was determined by the PVC tape adhered to either side of the 10mm exposed surface. The well for the cell was created by cutting down the sides of the border between the PVC tape and clear tape with a scalpel, leaving an uncut section of 0.5mm to the edge of the 10mm exposed area. The cut area was lifted from the surface and cut off, leaving a clear tape lip at the edge of the exposed area. The electrolyte well was sealed by coating silicone rubber, supplied by RS Components Ltd.

During the experiment, a humidity of 95% was used at a room temperature of 25˚C. The humidity was kept constant by placing reservoirs of 5% NaCl solution within the SKP chamber during the experiment. The sample was placed into the chamber and electrolyte was added to the silicone well to initiate the cathodic delamination process. The SKP chamber was closed to allow for the humidity to reach 95%. The SKP reference probe scanned, 100µm from the surface, 12mm lines along the coated PVB coated surface, starting from the defect edge. Scans were taken every 1h, and the Ecorr was recorded at 20 points per mm. Details on the SKP equipment and calibration have been described elsewhere. [17,18]

3. Results and Discussion

3.1 Surface appearance post uniaxial deformation

Fig.4 shows the surface morphology of ECCS post elongation at various percentage strains. Bands on the surface, forming at 45 degrees to the applied tension in the y-axis, intensify with increased strain. These surface features have been reported by X. Zhang, where they are identified as Lüders bands or localized areas of plastic deformation in the underlying steel substrate caused by discontinuous yielding [8]. No visual cracking is identified from

these band formations for ECCS samples. However the underlying substrate may still be exposed due to the formation of the slip bands cutting through the Cr layer. Defects seen on the surface are caused by the plating process and the penetration of features from the underlying steel. Elongation is not considered the cause for the discussed defects, due to the surface of 0% strain demonstrating similar imperfections. It may be assumed that these scratches are defects in the underlying steel, penetrating through the tin coating. ECCS does not show any cracks where the Lüders bands push through the surface. As ECCS is usually epitaxial to the substrate it may be assumed that they deform as one with the underlying steel. It is proposed that if no Cr is spread out over the surface during the process of straining, then it is expected no iron will be exposed at the features as long the steps in the y axis of the steel are smaller than the thickness of the Cr layer.

The SEM images in Fig.5-6 illustrate that the more deformation which is applied to the Cr(III) layer, for both the low (4mg/m^2) and high (19mg/m^2) Cr(III) oxide Cr(III) coatings, the more cracking appeared on the surface. Cracking on the outer surface of the samples appeared in bands, 45 degrees to the direction of force applied. The high Cr(III) oxide coating in comparison to the low Cr(III) oxide coating showed a higher value of interlinking smaller cracks, from the 45-degree bands. This feature could be attributed to the higher Cr(III) oxide content of 19mg/m^2, resulting in a higher degree of brittle cracking. Cracking of the coating however does not suggest the exposure of the underlying steel to a corrosive electrolyte due to the thickness of the oxide layer applied.

For low and high Cr(III) oxide coatings cracking formations are seen on the 5% strain samples. At 10% strain, little change is seen when compared to 5% strain for the low oxide coating. However for the high Cr(III) oxide coating visible cracks appear, due to the increased roughness caused by an increase in deformation. The amount of cracking increases between 10% and 20% for both samples; however, the cracks on the surface of the high Cr(III) oxide coating show regions of interlinking. A high density of tiny cracks are seen to cover the whole coating surface of the high oxide sample strained to 20%. The cracking is not only confined at the Lüders bands, but also is present in the areas between the features

The ECCS coating contains a defined chromium oxide and chromium metal layer. The chromium oxide layer will be damaged during deformation. However, oxidation of the chromium metal layer underneath to CrO_3 is suggested to repair the coating. The Cr(III) based coatings have no defined layers, where chromium oxide and chromium carbide are combined with chromium metal to form the coating. The formation of chromium oxide on a damaged Cr(III) coating will occur, comparable to ECCS, due to the oxidation of any exposed chromium metal after straining. The integration of chromium oxide and chromium carbide however may affect the ductility of the coating compared to a pure chromium metal layer. It is suggested that the ductility of the ECCS coating is higher compared to Cr(III) coatings, resulting in the presence of fewer cracks post uniaxial elongation. The impact of self-healing chromium oxidation properties is reduced for Cr(III) layers due to the absence of a pure chromium metal layer. ECCS has a lower coating weight compared to the Cr(III) coatings, therefore exposure of the substrate due to the formation of steps in the underlying steel, appears to be not directly related to the thickness of the coating. However the possibility that differences in coating weight, described in Table 1, contributes to the observed variations in behaviour cannot be ruled out.

3.2 Cathodic Disbondment

Initial experiments were completed on pure iron to acquire a threshold of resistance to delamination in the absence of the electroplated chromium coatings. From the point of initiation of the experiment, the PVB overcoat began to delaminate, resulting in the Ecorr(x) profiles shown in Fig.7(a). The intact coating values for Ecorr remained high and uniform at values between 0.05V and 0.22V vs SHE for 24 hours. Measured values are similar to studies previously completed [19]. At the point where the metal and electrolyte meet due to delamination, the Ecorr value drops to -0.25V vs SHE after initiation. The recorded value is expected and in the region of active anodic iron at -0.44V vs SHE [15,19].

Previous studies have shown that a local cathode is established during the delamination of the PVB layer [16]. This local cathode supports the oxygen reduction reaction, which is

found at the delamination front and results in a loss of adhesion between the coating layer and the substrate. The coating defect exhibits anodic dissolution of iron. The link between the anodic and cathodic sites causes an ionic current to flow underneath the PVB film. Ingress of the electrolyte from the defect to the cathodic delamination front occurs leading to coating disbondment as the electrolyte progresses further from the defect. Due to the ionic conductivity of the electrolyte, a linear gradient in potential is established between the E_{corr} at the cathode and the still intact PVB coating. The maximum gradient in the E_{corr} profiles has been shown as a semi-empirical method of determining the delamination front [16,19]. On iron, as the delamination front moves further from the defect site, the rate of any further delamination decreases with time. This phenomenon is found on systems where the delamination is controlled by the migration of ions from the defect site to the cathodic front. In the case of this experiment, the migration of electrolyte cations (Na^+). For migration controlled delamination, the time since the introduction of electrolyte (tdel), is related to the distance of delamination (xdel), where t_i is the initiation period, and kd is the rate of delamination [19,21].

$$x_{del} = k_d(t_{del} - t_i)^{1/2}$$

A plot of xdel vs (t_{del} - t_i) for iron Ecorr profiles were compiled and shown in Fig 7(b). The plot shows a parabolic curve identifying migration controlled disbondment kinetics [21].

Three repeats were completed on the four ECCS samples, 0%, 5%, 10% and 20% strain, which resulted in no cathodic delamination over a time of 96 hours. The Ecorr values remained level shown in Fig. 8, due to no coupling between the defect and a cathodic delamination front, even at the highest elongation of 20%. Throughout the experiment, the Ecorr value for an intact coating was measured.

Cathodic delamination was observed for both the low ($4mg/m^2$) and high ($19mg/m^2$) Cr(III) oxide Cr(III) coating samples, however, at different values of elongation. The high Cr(III) oxide coating at 0% and 5% elongation observed the same Ecorr potential plateau shown for all the ECCS samples, indicating no cathodic delamination over 96 hours. Fig.9 shows the $E_{corr}(x)$ profiles for 10% strain, high Cr(III) oxide coating, which are displayed from initiation time, followed by 4-hour gaps, over 24 hours of delamination. The data shows that the $E_{corr}(x)$ profiles are separated by a constant distance over the length of the

delamination experiment, suggesting linear kinetics controlled by electron transfer [21]. Electron transfer controlled delamination of a PVB overcoat on Cr(III) coatings have been shown by Wint [1]. Wint suggested delamination initiated on Cr(III) based coatings due to pinholes observed on scanning electron microscope images. The pinholes were suggested to expose the underlying steel, acting as defects in the coating. The high Cr(III) oxide coating showed no delamination when no deformation was applied. Therefore the only defects in the coating are the cracks formed post-deformation. Fig. 10 shows plots of delamination area vs time for 10% and 20% strain, high Cr(III) oxide coating. An increase in the delamination distance from 850µm to 1050µm occurs at a higher strain percentage. Differences between the intact and delaminated potential values are not present between the two deformed samples.

The low Cr (III) oxide (4mg/m^2), Cr(III) coating sample, when no deformation has been applied, observes cathodic disbondment of the PVB overcoat. The Ecorr profiles, shown in Fig.11, are separated by constant intervals, similar to the deformed high Cr(III) oxide coating, suggesting electron transfer controlled disbondment. The delamination distance for 0% strain low Cr (III) oxide coating was greater than 20% strain high Cr (III) oxide coating, over 24 hours from initiation, with an increase of 1200µm. Plots of delamination distance vs time (Fig.12) show more significant differences between 0% and 5% strain, compared to the 5% increases between the three deformed low Cr (III) oxide samples. The cathodic disbondment distances remain within 750 µm, compared to the 1400 µm distance between 0% and 5% strain. The cathodic dibondment results discussed for the low Cr (III) oxide coating, suggest that once the coating has cracked at 5% strain, any further increase in deformation has a reduced effect. The time taken for the high Cr (III) oxide coatings to initiate delamination of the PVB layer was much higher than of the low Cr (III) oxide coatings (Table 3).

An increase in delamination rates is seen for increased deformation levels for both low (4mg/m^2) and high (19mg/m^2) Cr(III) oxide coatings. However, ECCS shows no delamination of the PVB overcoat up to 20% uniaxial strain. Potentials at the intact interface are much higher for Cr(III) based coatings than for ECCS, which is an indication for the oxygen reduction reaction (ORR) reactivity on the surface [22]. The images of the

three samples, deformed to different levels of strain, show increases in surface cracking for both Cr(III) based coating samples but not ECCS. The increase in cracking is suggested to be caused by the presence of chromium oxide and chromium carbide in the chromium metal layer, reducing the barrier properties of the Cr(III) based coating. Therefore, a relationship can be proposed between deformation induced cracking and cathodic disbondment of a polymer overcoat for coatings of identical composition. Delamination has been shown to increase on Cr(III) coatings with the equivalent chromium oxide levels, as the percentage of strain increases. The studies completed suggests that higher Cr(III) oxide levels reduce the rate of delamination for undeformed and deformed Cr(III) based coating. Chromium oxide behaves like an electrical insulator due to its wide-bandgap semiconductor properties. It is determined that chromium oxide would alter the rate-determining step of cathodic disbondment by decreasing the rate of electron transfer across the surface of the coating [23, 24]. Studies completed by Boelen del [14]. report a reduction in underfilm corrosion and blistering of PET coated ECCS DRD cans with increased chromium oxide levels. The effect of chromium oxide levels on reducing cathodic disbondment rates remains present post uniaxial deformation of the coating.

Table 3. Initiation times of PVB film cathodic disbondment on Cr(III) based coatings.

Sample	Initiation Time (mins)
High Cr(III) oxide (19mg/m^2) Cr(III) coating 10% Strain	5040
High Cr(III) oxide (19mg/m2) Cr(III) coating 20% Strain	5100
Low Cr(III) oxide (4mg/m^2) Cr(III) coating 0% Strain	2800
Low Cr(III) oxide (4mg/m^2) Cr(III) coating 5% Strain	3180

Low Cr(III) oxide (4mg/m^2) Cr(III) coating 10% Strain	3600
Low Cr(III) oxide (4mg/m^2) Cr(III) coating 20% Strain	3000

3.3 Hydrogen Evolution

Potentiodynamic scans on ECCS and Cr(III) coating samples were conducted in a sodium sulphate solution, buffered to pH 9.3 at 20^{o}C. Deareated conditions were used to suppress the oxygen reduction reaction and measure the true, current value for hydrogen evolution. Fig.13 shows current density values recorded at a potential of -1.1V vs SHE. The potential chosen was in the cathodic hydrogen evolution region [27]. When the strain percentage is increased for ECCS samples, the cathodic current density value does not increase with deformation. The values remain between -2.80E-05 and -3.41E-05 A.cm^{-2}. The result indicates the coating remains intact post strain. Due to the electrochemical availability of iron compared to chromium, a defect in the coating exposing the underlying steel substrate would produce higher cathodic current value for hydrogen evolution.

The hydrogen evolution cathodic current values increased with strain for both high and low Cr(III) oxide Cr(III) coatings. Deformed high Cr(III) oxide samples increased gradually from -1.10E-05 to -1.13E-03 A.cm^{-2} as the strain percentage increased. Cracking can be observed on Fig.5-6., which suggests as the samples are deformed to a higher degree, the electrochemical availability of the iron increases. The low Cr(III) oxide coating shows the same trend as high Cr(III) oxide coating, however to a greater extent, with the sample deformed to 20% strain, producing a value of -3.81E-03 A.cm^{-2}. It is proposed that the Cr(III) oxide levels suppress the cathodic hydrogen evolution reaction, even when the coating is defected by deformation and exposure of the substrate occurs. A thicker oxide layer should cause a more brittle behavior and hence intuitively more cracking and more exposed Fe. This however has shown not to be the case, as seen in Fig.13. Thus it would seem that, over the range of thicknesses studied, iron exposure on deformation is not strongly dependent on Cr(III) oxide thickness.

Tafel slopes for the hydrogen evolution reaction for Fe and low (4mg/m^2) Cr(III) oxide coating, with 0% and 20% applied uniaxial strain are shown in Fig 14. The Tafel slopes values are shown in Table 4. for all samples. A mechanistic hydrogen evolution reaction occurs in the following steps [25]:

1. $H_3O^+ + e- + M - \sim M- H + H_2O$ (Volmer reaction)
   Followed by
2. $H_3O^+ + e- + M\text{--}H \sim M + H_2 + H_2O$ (Heyrovsky reaction)

Or

3. $2M\text{-}H \sim 2M + H_2$ (Tafel reaction)

The results of ECCS and Cr(III) based coatings do not follow this theory where the rate determining step is Volmer, Heyrovsky or Tafel reactions. This is due to the coatings having a layer of chromium oxide present on the surface, producing a non-mechanistic Tafel slope. The Cr oxide layer on ECCS and the Cr(III) coatings results in higher Tafel slope values of between -281mV/dec to -490mV/dec, compared to a typical hydrogen evolution reaction at 120mV/dec, where the electrons exchanged is equal to 1, assuming the charge transfer coefficient is 0.5. [24,25]. A drop in Tafel slope values due to the removal of an oxide film has been studied and explained by Azzerri [24], where studies obtained a Tafel slope value of -260mv/dec for chromium coated tin-free steel (TFS), similar to the measured -286 mv/dec for non-deformed ECCS . The dual barrier model developed by Meyer has been utilised to explain the effects a thin oxide layer has on the hydrogen evolution reaction kinetics [25,28]. Meyer explains that two barriers are kinetically significant for oxide covered metals.

i) The Helmholtz double layer must be overcome by the charge carriers, H_30^+
ii) A potential energy barrier within the oxide must be negotiated by the electrons from the metal surface, to reach the interface between the oxide and solution, where neutralization of the charge carriers H_30^+ and e^- occurs.

[27]

Azzerri [25] concluded that for chromium coated steels in deaerated, the mechanism could be based on Langmuir adsorption of hydrogen atoms, with the rate determining step as electrochemical desorption and the dual barrier model.

The Tafel slope result for Fe in a sodium sulphate solution, buffered to pH 9.3, was -146 mv/dec. Studies by María R. Gennero de Chialvo and Abel C. Chialvo [29] recorded a similar result of -133.2 mv/dec in alkaline conditions.

The cause for the increase in measured hydrogen evolution current density on Cr(III) based coatings, when the strain is increased, is suggested to be caused by an increase in the availability of iron. It is proposed that the increase in hydrogen evolution levels can be related to an increase in the exposure of iron caused subjecting the samples to higher levels of uniaxial deformation. At 20% elongation, both high and low Cr(III) oxide coatings show a change in Tafel slope values in the direction of the measured Tafel slope value for Fe. It is not possible to estimate oxygen reduction current densities directly from the observed hydrogen evolution current densities. However, it is reasonable to assume that both hydrogen evolution and oxygen reduction will occur on the surface of the steel substrate where it is exposed through cracks in the Cr(III) coating. As such, the observed hydrogen evolution current is a measure of the fraction of the sample surface which is electrochemically available to support cathodic activity (whether that is cathodic hydrogen evolution or oxygen reduction). Increasing coating wt% might reasonably be expected to decrease cathodic activity and delamination rates in undeformed samples. However, it is less obvious that increased coating wt% would make the coatings more resistant to cracking on deformation. All else being equal thicker coatings would tend to be more rigid and so more likely to crack under straining.

Sample	Uniaxial Elongation %	Cathodic Tafel slope, mv/decade
Fe	0	-146
Low Cr(III) oxide (4mg/m^2) Cr(III) coating	0	-490
	5	-436
	10	-442
	20	-302
High Cr(III) oxide (19mg/m^2) Cr(III) coating	0	-470
	5	-459
	10	-442
	20	-360
ECCS	0	-286
	5	-281
	10	-292
	20	-288

Table 4 Values of the experimental kinetic for ECCS, Cr(III) coatings and Fe in 0.5M Na2SO4 buffered to pH 9.3

4. Conclusion

A study of corrosion and surface morphology was completed on coatings from Cr(VI) (ECCS) and Cr(III) based electrolyte baths. Two Cr(III) based coatings were used, containing different levels of Cr(III) oxides, 4mg/m^2 and 19mg/m^2.

The ECCS coating was fully resistant to corrosion driven disbondment in non-deformed and deformed states. At all strain percentages, no cathodic disbondment occurred, along with no changes in hydrogen evolution current density values. SEM images taken of the surface at varying levels of deformation, illustrated no cracking of the surface, suggesting a ductile coating.

High (19mg/m2) levels of Cr (III) oxide, observed cathodic driven disbondment of the PET coating post-deformation. The delamination rates increased when the strain applied was raised over 10%. Both 0% and 5% strain samples remained resistant to disbondment. Low (4mg/m2) levels of Cr(III) oxide, showed cathodic disbondment for non-deformed and deformed coatings. Higher disbondment rates are observed from 0% to 5% strain compared to TH; however, further deformation does not increase the rate at the same factor. The kinetics of the delamination measured were found to be electron transfer controlled due to the linear nature of the cathodic delamination rates. It is proposed that difference in PVB disbondment for both Cr(III) based coatings is due to the reduced electron transfer rates across the surface with increased chromium oxide levels, due to its semiconductor properties. Scanning electron microscope (SEM) studies found an increase in surface cracking when the strain applied was increased for both Cr(III) based coating samples. Measured hydrogen evolution rates for varying strain percentages, showed an increase in the cathodic current density values as the strain percentage increased for Cr(III) based coatings. Higher cathodic values of current density for hydrogen evolution were observed for the low Cr(III) oxide (4mg/m^2) samples in non-deformed and deformed states.

An argument is presented that deformation influences the corrosion performance of Cr(III) based coatings. Previous studies have shown comparable results between ECCS and Cr(III) coatings, however post straining Cr(III) coatings behaves in a way which is significantly

different from what has previously been observed for ECCS like coatings [1-2,9-10]. It is proposed that the increase in hydrogen evolution levels can be related to an increase in the exposure of iron due to the cracking formations found on the surface of identical Cr(III) coatings. The cracking shown on the surface of the chromium coated steel is suggested to cause the increase in cathodic disbondment rates found during the SKP investigations. Cracking of the surface and exposure of iron is suggested to allow for a continuous cathodic front, causing ingress of electrolyte underneath the PVB model coating. Higher Cr oxide levels are suggested to suppress both cathodic driven disbondment and the hydrogen evolution reaction, even when the coating has deformation induced defects.

Author Declaration

We wish to draw the attention of the Editor to the following facts regarding financial support for this work and the interests of any authors:

The work contained within the manuscript was funded by The Engineering and Physical Sciences Research Council, by TATA Steel Europe and part-funded by the European Social Fund through the Welsh European Funding Office.

We would like to disclose that the second author, Dr. Arnoud de Vooys is a principal researcher at TATA Steel Research and Development Technology Centre.

We confirm that the manuscript has been read and approved by all named authors and that there are no other persons who satisfied the criteria for authorship but are not listed. We also confirm that the order of authors listed in the manuscript has been approved by all of us.

We confirm that we have given due consideration to the protection of intellectual property associated with this work and that there are no impediments to publication, including the timing of publication, with respect to intellectual property. In doing so we confirm that we have followed the regulation of our institutions concerning intellectual property.
We understand that the Corresponding Author is the sole contact for the Editorial process (including Editorial Manager and direct communications with the office. He is responsible for communicating with the other authors about progress, submissions of revision and final approval

of proofs. We confirm that we have provided a current, correct email address which is accessible by the Corresponding Author and which has been configured to accept email.

CRediT authorship contribution statement

J.Whiteside: Conceptualization, Formal analysis, Investigation, Methodology, Write – original draft. H.N. McMurray: Conceptualization, Methodology, Writing – review and editing, Supervision. E.Sackett: Methodology, Writing – review and editing, Supervision. A.C.A. deVooys: Supervision, Resources, Writing – review and editing.

Data availability statement

The raw/processed data required to reproduce these findings cannot be shared at this time as the data also forms part of an ongoing study.

Acknowledgements

The authors would like to thank TATA Steel and for financial support by EPSRC (EP/L015099/1) and the Materials and Manufacturing Academy (M2A). The work was further supported by the Advanced Imaging of Materials (AIM) Facility at Swansea University, funded in part by the EPSRC (EP/M028267/1) and the European Regional Development Fund through the Welsh Government (80708)

References

[1] Wint, N., de Vooys, A.C.A. and McMurray, H.N., 2016. The corrosion of chromium based coatings for packaging steel. Electrochimica acta, 203, pp.326-336.

[2] Edy, J.E., McMurray, H.N., Lammers, K.R. and Arnoud, C.A., 2019. Kinetics of corrosion-driven cathodic disbondment on organic coated trivalent chromium metal-oxide-carbide coatings on steel. Corrosion Science, 157, pp.51-61.

[3] Mora, N., Cano, E., Bastidas, J.M., Almeida, E. and Puente, J.M., 2002. Characterization of passivated tinplate for food can applications. Journal of Coatings Technology, 74(935), pp.53-58.

[4] Katz, S.A. and Salem, H., 1993. The toxicology of chromium with respect to its chemical speciation: a review. Journal of Applied Toxicology, 13(3), pp.217-224.

[5] Langård, S. and Norseth, T., 1975. A cohort study of bronchial carcinomas in workers producing chromate pigments. Occupational and Environmental Medicine, 32(1), pp.62-65.

[6] Rees, I.S., 1998. EUR 17860 Properties and in service performance. Development of chromium free passivation films for tin plate, Office for Official Publications of European Communities, Luxembourg

[7] Wijenberg, J.H.O.J., Steegh, M., Aarnts, M.P., Lammers, K.R. and Mol, J.M.C., 2015. Electrodeposition of mixed chromium metal-carbide-oxide coatings from a trivalent chromium-formate electrolyte without a buffering agent. Electrochimica Acta, 173, pp.819-826.

[8] Wijenberg, J.H.O.J., Tata Steel Ijmuiden BV, 2014. Method for manufacturing chromium-chromium oxide coated substrates.

[9] Boelen, B., den Hartog, H. and van der Weijde, H., 2004. Product performance of polymer coated packaging steel, study of the mechanism of defect growth in cans. Progress in organic coatings, 50(1), pp.40-46.

[10] Zhang, X., Boelen, B., Beentjes, P., Mol, J.M.C., Terryn, H. and De Wit, J.H.W., 2007. Influence of uniaxial deformation on the corrosion performance of pre-coated packaging steel. Progress in organic coatings, 60(4), pp.335-342.

[11] De Vooys, A.C.A., Boelen, B. and Van Der Weijde, D.H., 2012. Screening of coated metal packaging cans using EIS. Progress in Organic Coatings, 73(2-3), pp.202-210.

[12] Bastos, A.C. and Simões, A.M.P., 2003. Effect of uniaxial strain on the protective properties of coil-coatings. Progress in organic coatings, 46(3), pp.220-227.

[13] de Vooys, A. and van der Weijde, H., 2011. Investigating cracks and crazes on coated steel with simultaneous SVET and EIS. Progress in Organic Coatings, 71(3), pp.250-255.

[14] Boelen, B., 2009. The influence of deformation on the product performance of pre-coated packaging steels.

[15] Posner, R., Fink, N., Giza, G. and Grundmeier, G., 2014. Corrosive delamination and ion transport along stretch-formed thin conversion films on galvanized steel. Surface and Coatings Technology, 253, pp.227-233.

[16] Leng, A., Streckel, H. and Stratmann, M., 1998. The delamination of polymeric coatings from steel. Part 1: Calibration of the Kelvinprobe and basic delamination mechanism. Corrosion Science, 41(3), pp.547-578.

[17] Williams, G. and McMurray, H.N., 2001. Chromate inhibition of corrosion-driven organic coating delamination studied using a scanning Kelvin probe technique. Journal of the Electrochemical Society, 148(10), p.B377.

[18] Williams, G., McMurray, H.N. and Worsley, D.A., 2001. Latent fingerprint detection using a scanning Kelvin microprobe. Journal of Forensic Science, 46(5), pp.1085-1092.

[19] Holness, R.J., Williams, G., Worsley, D.A. and McMurray, H.N., 2005. Polyaniline inhibition of corrosion-driven organic coating cathodic delamination on iron. Journal of the Electrochemical Society, 152(2), p.B73.

[20] Stratmann, M., Feser, R. and Leng, A., 1994. Corrosion protection by organic films. Electrochimica Acta, 39(8-9), pp.1207-1214.

[21] Leng, A., Streckel, H. and Stratmann, M., 1998. The delamination of polymeric coatings from steel. Part 2: First stage of delamination, effect of type and concentration of cations on delamination, chemical analysis of the interface. Corrosion Science, 41(3), pp.579-597.

[22] Hausbrand, R., Stratmann, M. and Rohwerder, M., 2008. The physical meaning of electrode potentials at metal surfaces and polymer/metal interfaces: consequences for delamination. Journal of the Electrochemical Society, 155(7), p.C369.

[23] Abdullah, M.M., Rajab, F.M. and Al-Abbas, S.M., 2014. Structural and optical characterization of Cr2O3 nanostructures: Evaluation of its dielectric properties. Aip Advances, 4(2), p.027121. [23] Rivera, R. et al., 2013. Quantum Chemical Study of Defective Chromium Oxide. , II, pp.4–8.

[25] Azzerri, N., 1975. Kinetics of the hydrogen evolution reaction on chromium, chromium oxide coated steel. Journal of Electroanalytical Chemistry and Interfacial Electrochemistry, 66(2), pp.99-110.

[26] Popić, J.P. and Dražić, D.M., 2004. Electrochemistry of active chromium: Part II. Three hydrogen evolution reactions on chromium in sulfuric acid. Electrochimica acta, 49(27), pp.4877-4891.

[27] Pourbaix M. Atlas of electrochemical equilibria in aqueous solutions. 2nd ed. Houston: National Association of Corrosion Engineers, 1974 (p. 226).

[28] Meyer, R.E., 1960. Cathodic processes on passive zirconium. Journal of The Electrochemical Society, 107(10), p.847.

[29] de Chialvo, M.R.G. and Chialvo, A.C., 2001. Hydrogen evolution reaction on a smooth iron electrode in alkaline solution at different temperatures. Physical Chemistry Chemical Physics, 3(15), pp.3180-3184.

List of figures

Figure 8 SKP derived Ecorr vs distance (x) profiles for ECCS with a 30 µm PVB film, held in air at 95% R.H., initiated using 0.86 mol.dm^3 NaCl (aq.) applied to a penetrative coating defect.

Figure 9 SKP derived Ecorr vs distance (µm) profiles for high Cr(III) oxide (19mg/m^2) Cr(III) coating overcoated with a 30 µm PVB film, held in air at 95% R.H., initiated using 0.86 mol.dm3 NaCl applied to a penetrative coating defect. Starting at 5040 mins, 2-hour intervals thereafter.

Figure 10 Plots of delamination distance (xdel) vs time obtained for high Cr(III) oxide (19mg/m^2) Cr(III) coating, uniaxial strain 10% (●) and 20% (◥), overcoated with a 30 mm PVB film where corrosion was initiated using a 0.86 mol.dm3 NaCl electrolyte.

Figure 11 SKP derived Ecorr vs distance (x) profiles for low Cr(III) oxide (4mg/m2) Cr(III) coating, overcoated with a 30 µm PVB film, held in air at 95% R.H., initiated using 0.86 mol.dm3 NaCl (aq.) applied to a penetrative coating defect. Starting at 2800 mins, 2-hour intervals thereafter.

Figure 12 Plots of delamination distance (xdel) vs time obtained for low Cr(III) oxide (4mg/m2) Cr(III) coating, uniaxial strain 0% (▼), 5% (■), 10% (●) and 20% (▲), overcoated with a 30 mm PVB film where corrosion was initiated using a 0.86 mol.dm3 NaCl electrolyte.

Figure. 13 Cathodic polarisation, current density vs uniaxial strain % of deformed low Cr(III) oxide (4mg/m2) (●), high Cr(III) oxide (19mg/m^2) (■) Cr(III) coatings and ECCS (▲) in a deaerated 0.5M Na2SO4 buffered to pH 9.3 Potential sweep rate 3.3 × 10−4 Vs-.

Figure. 14 Tafel plots of pure iron (▲) and low Cr(III) oxide (4mg/m2) Cr(III) coating, uniaxial strain 0% (■) and 20% (●) in a deaerated 0.5M Na2SO4 buffered to pH 9.3. Potential sweep rate 3.3 × 10−4 Vs−1.

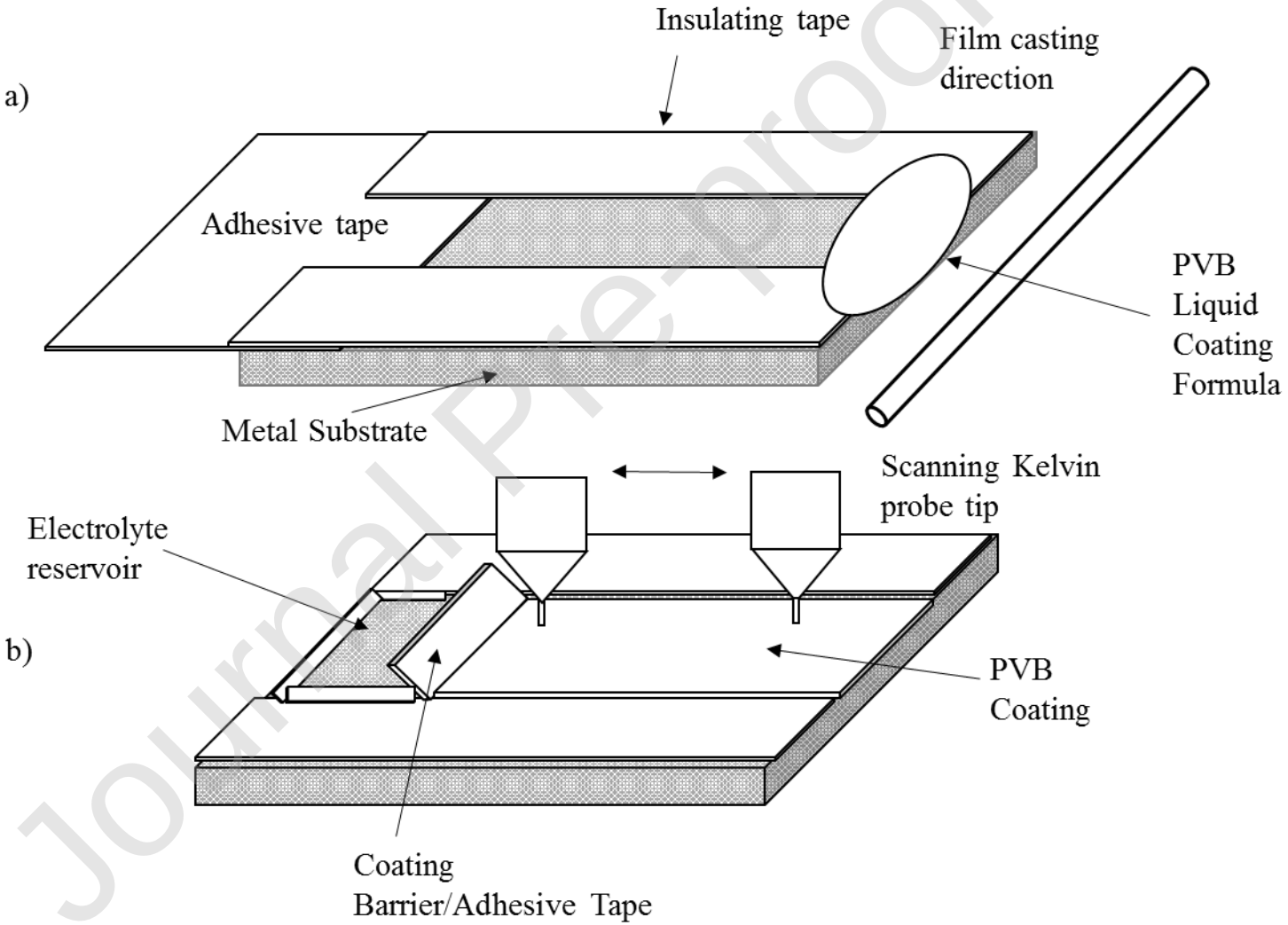

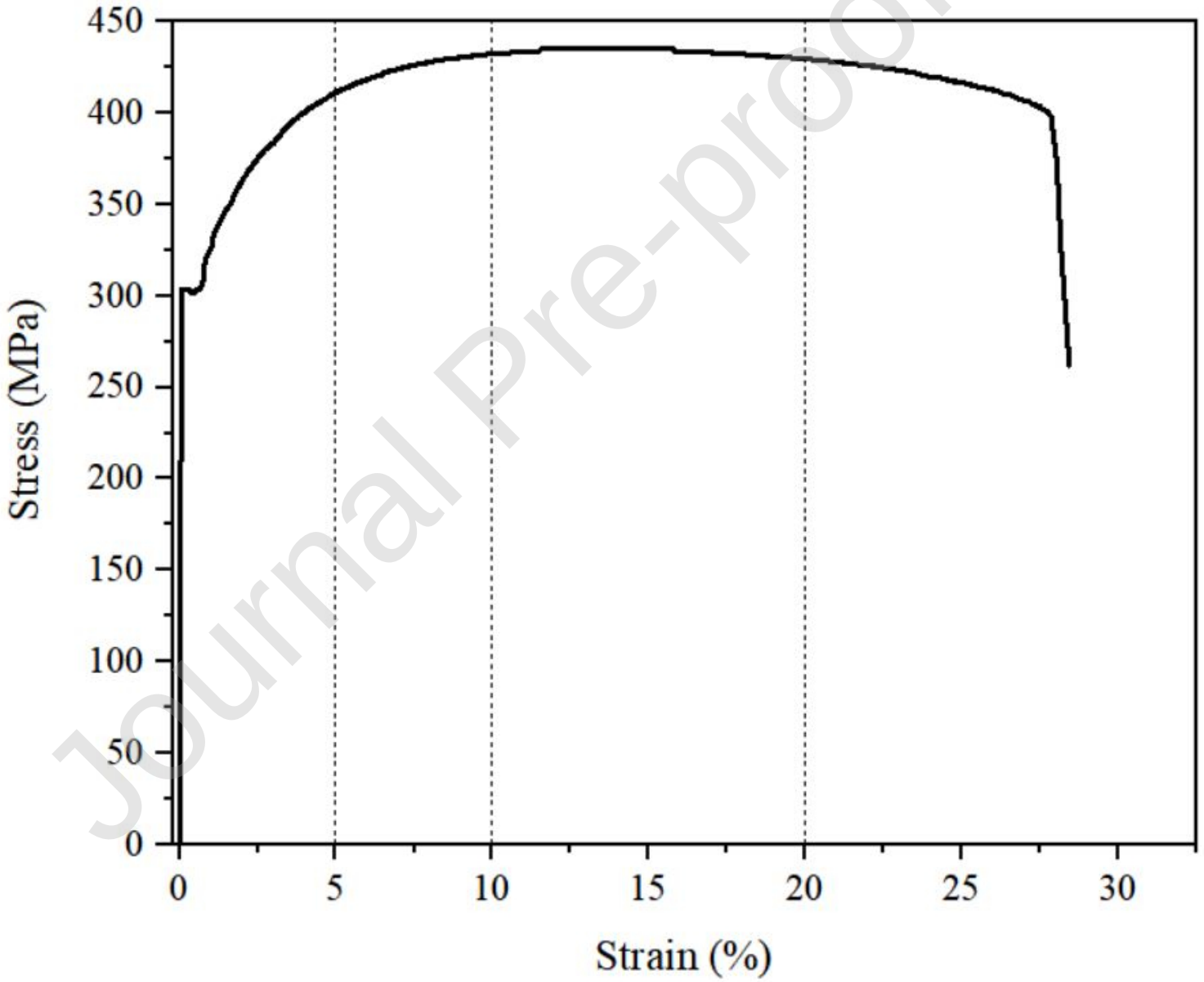

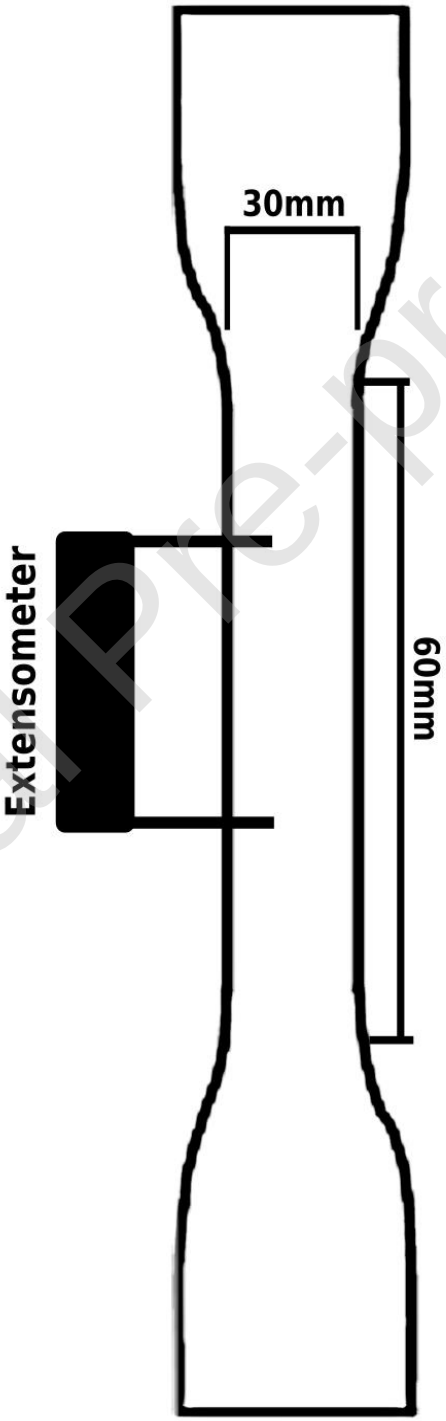

a)

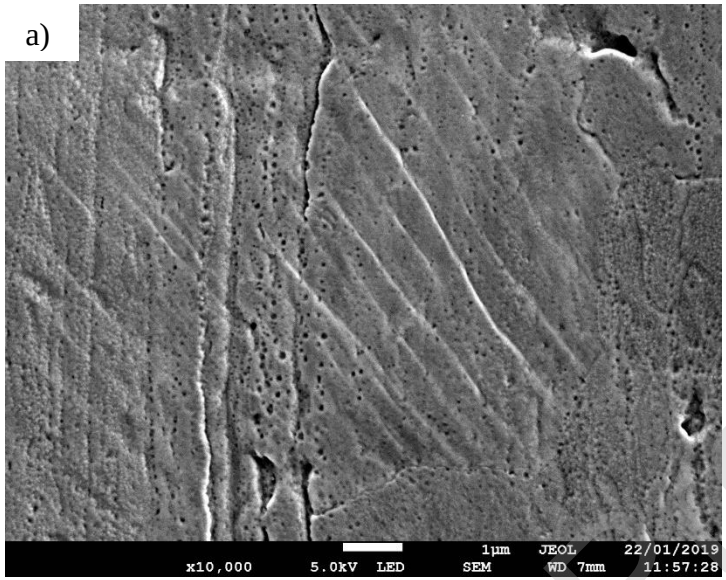

b)

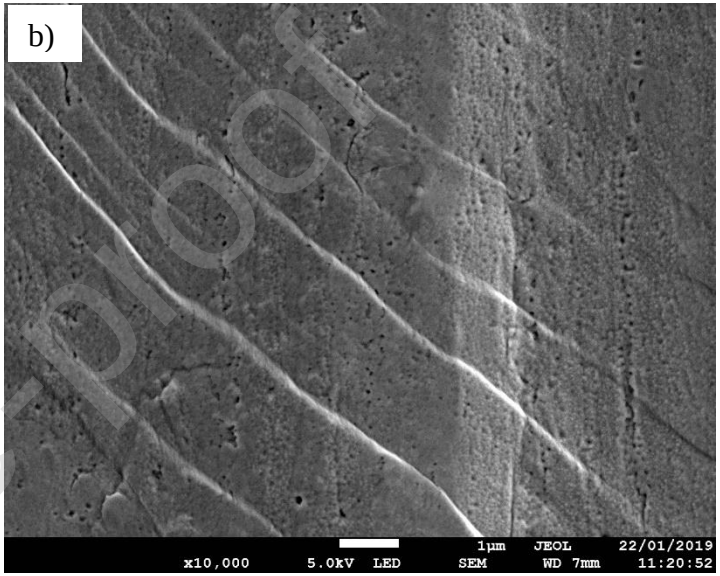

c)

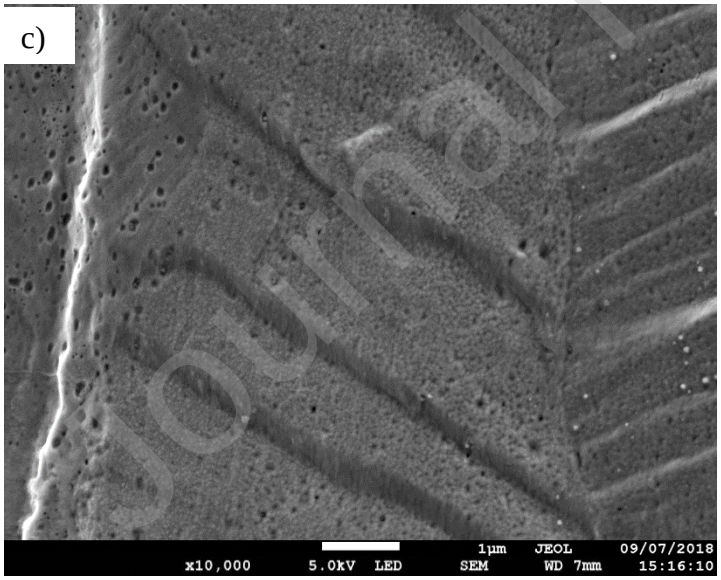

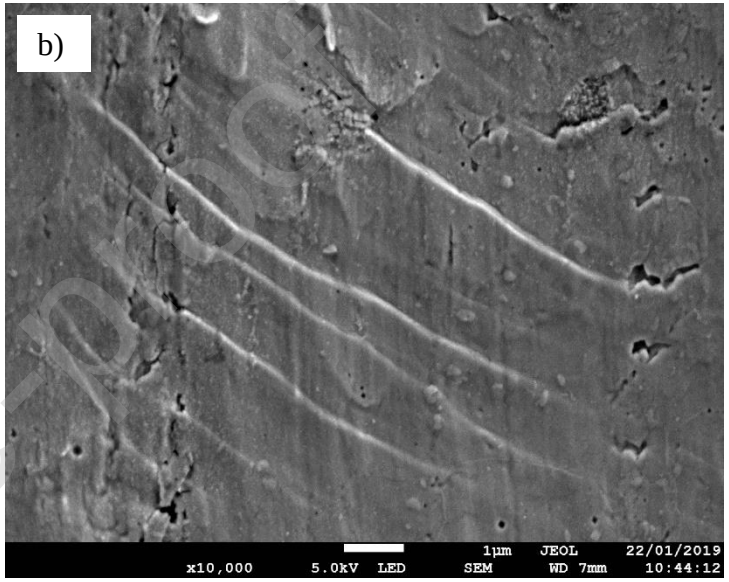

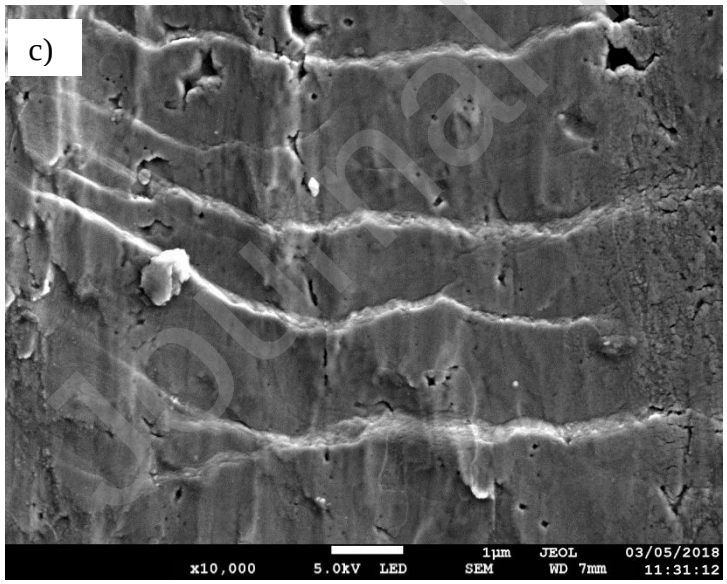

a)

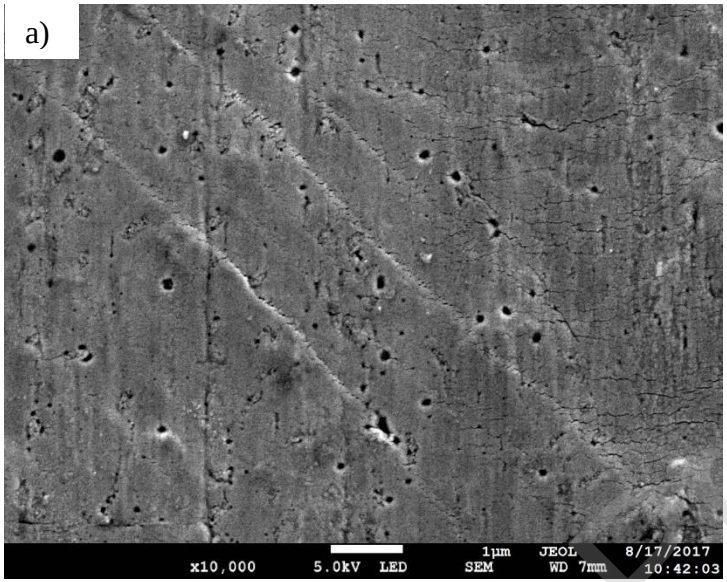

b)

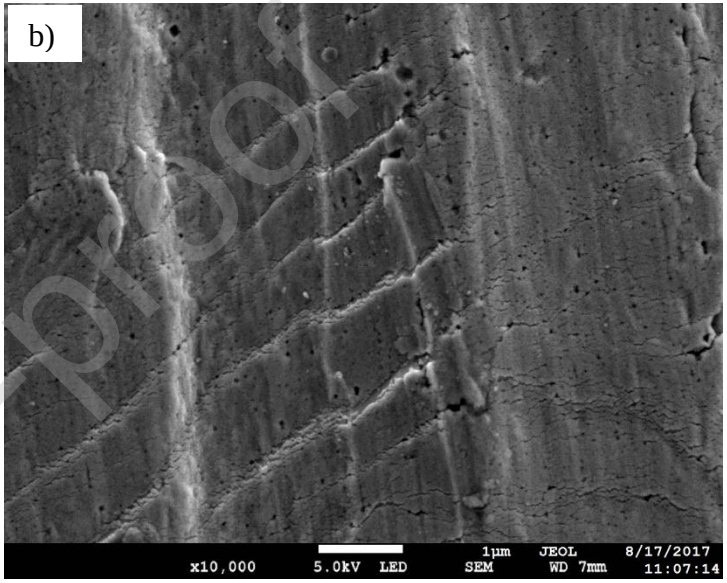

c)

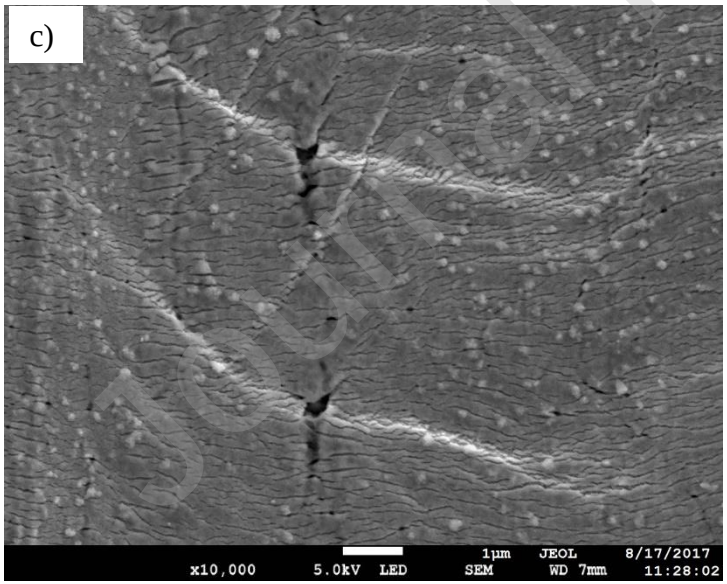

(a)

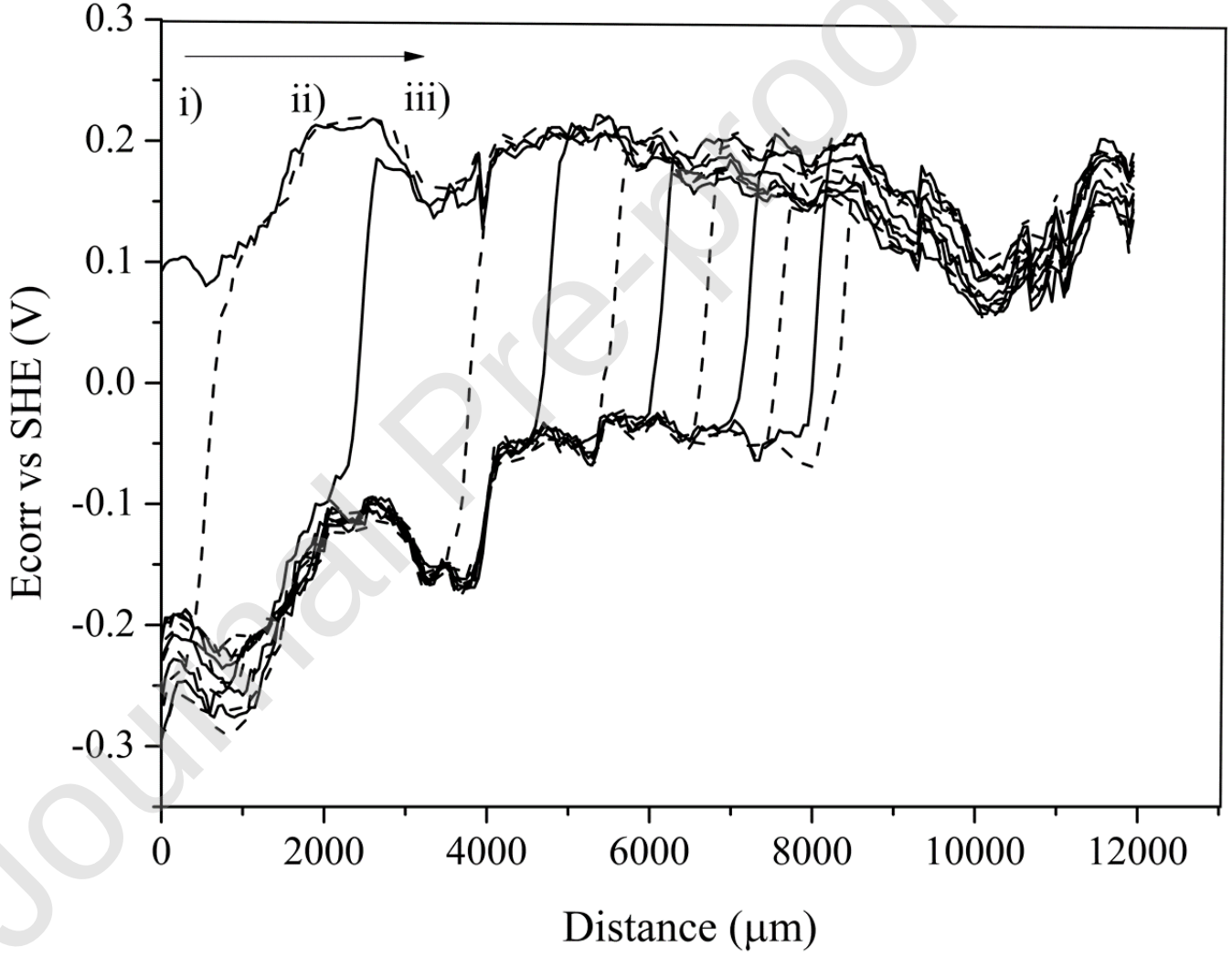

(b)